

^{68}Ga -FAPI PET visualize heart failure: from mechanism to clinic

Wenyu Song

Union Hospital, Tongji Medical College, Huazhong University of Science & Technology

Xiao Zhang

Union Hospital, Tongji Medical College, Huazhong University of Science & Technology

ShuKun He

Union Hospital, Tongji Medical College, Huazhong University of Science & Technology

Yongkang Gai

Union Hospital, Tongji Medical College, Huazhong University of Science & Technology

Chunxia Qin

Union Hospital, Tongji Medical College, Huazhong University of Science & Technology

Fan Hu

Union Hospital, Tongji Medical College, Huazhong University of Science & Technology

Yan Wang

Union Hospital, Tongji Medical College, Huazhong University of Science & Technology

Zhaohui Wang

Union Hospital, Tongji Medical College, Huazhong University of Science & Technology

Peng Bai

Union Hospital, Tongji Medical College, Huazhong University of Science & Technology

Jing Wang

Union Hospital, Tongji Medical College, Huazhong University of Science & Technology

Xiaoli Lan (✉ xiaoli_lan@hust.edu.cn)

Department of Nuclear Medicine, Union Hospital, Tongji Medical College, Huazhong University of Science & Technology


<https://orcid.org/0000-0002-7263-7399>

Research Article

Keywords: heart failure, ^{68}Ga -FAPI, FAP, myocardial fibrosis, PET

Posted Date: August 23rd, 2022

DOI: <https://doi.org/10.21203/rs.3.rs-1953463/v1>

License:  This work is licensed under a Creative Commons Attribution 4.0 International License. [Read Full License](#)

Abstract

Purpose

Heart failure (HF) is a chronic and progressive clinical syndrome with structure or functional abnormalities of the heart. Active fibroblasts and ventricular remodeling play an essential role in the progression of HF. ^{68}Ga -labeled fibroblast activating protein inhibitor (^{68}Ga -FAP) have been proved binding with fibroblast activation protein (FAP) in many diseases. This study aimed to use ^{68}Ga -FAP PET to continuously visualize the dynamic change process of cardiac fibroblasts and HF to aid in the clinical management of HF.

Methods

The rat model of HF was established by injection of isoproterenol for 14 d continuously. Echocardiography and ^{68}Ga -FAP were performed weekly. Isolated hearts were taken every week for biodistribution, autoradiography, hematoxylin-eosin, FAP-immunofluorescence and Masson's trichrome staining, and blood samples for enzyme-linked immunosorbent assay. A preliminary study of HF patients further recruited for ^{13}N -amino (^{13}N - NH_3) perfusion and ^{68}Ga -FAP cardiac PET imaging simultaneously.

Results

Extensive myocardial uptake of ^{68}Ga -FAP, expression of FAP, and myocardial contractility peaked at 7 d after the onset of modeling, while only slight fibrotic changes were manifested. With time extension, ^{68}Ga -FAP uptake and ventricular wall motion of the heart reduced, while cardiac fibrosis and degree of myocardial injury gradually increased. Seven patients diagnosed with HF were successfully enrolled (5 men and 2 women, 58.14 ± 16.25 years). ^{13}N - NH_3 perfusion was inconsistent with ^{68}Ga -FAP uptake. Higher myocardial ^{68}Ga -FAP uptake was demonstrated in the patients with < 1-year duration than other groups.

Conclusion

With the progress of HF, ^{68}Ga -FAP accumulates evidently in the early stage, and gradually reduced. Preliminary clinical study suggested that ^{68}Ga -FAP PET could be used to display active fibrosis. Active myocardial FAP expression is followed by myocardial remodeling and myocardial fibrosis, suggesting that the detection of early active FAP expression may help guiding antifibrotic-drug therapy.

Clinical Trial Registration

NCT04982458

Introduction

Heart failure (HF) is a chronic and progressive clinical syndrome in which the heart structure or function is abnormal due to multiple factors [1]. It is a global disease, affecting at least 64.3 million people worldwide, and the prevalence is rising [2]. As the disease progresses, the survival rate of patients with HF gradually decreased, which is comparable to that of most malignancies [3]. The mortality rate is similar to prostate and colorectal cancer in men, as well as breast and ovarian cancer in women [4]. In this scenario, HF could be named as "malignancy" in the cardiovascular field. It is necessary to monitor the progress of HF and detect the factors related to this process, so as to formulate strategies to ensure the best cost-effectiveness of patient care [5].

Fibrosis is observed in nearly every form of myocardial disease [6]. Upon the injury of the heart, cardiac fibroblasts (CF) begin to remodel the myocardium *via* extracellular matrix (ECM) deposition, resulting in increased tissue stiffness and reduced compliance [7, 8]. Excessive CF is an important factor in the progression of HF [9]. Currently, the evaluation of CF mainly includes endomyocardial biopsy, and magnetic resonance imaging (MRI) [10]. Endomyocardial biopsy is limited by its invasiveness, and MRI is inadequate to detect pathological cardiac fibroblasts in early phase. Excitedly, fibroblast activation protein (FAP), which is robustly expressed in activated cardiac fibroblasts and minimally expressed in normal hearts [11], has been a potential and early candidate for targeting of pathological cardiac fibroblasts and the progression of HF.

There have limited clinical interventions and therapies for CF [12]. Angiotensin-receptor-neprilysin inhibitor (ARNI) has also been confirmed to improve ventricular remodeling and thus delay the progression of fibrosis [13]. Some novel therapy drugs or methods are in the line for clinical studies or trials, including pirfenidone [14] and engineered T cells [15]. Before therapy, early and precision identification

of CF is important for clinical management, and more meaningfully, FAP quantitation may provide information for the degree of activated fiber expression, and evaluate the therapeutic effect objectively.

Currently, ^{68}Ga -labeled fibroblast activating protein inhibitor (^{68}Ga -FAP), as a novel but outstanding target to FAP, has been proved to display the activated fibroblast response noninvasively with the advantage of a high target to background ratios [16, 17]. At present, several studies showed that ^{68}Ga -FAP could visualize the fibrosis process of the lung and liver [18]. FAP expression in acute myocardial infarction has also been observed by ^{68}Ga -FAP [19]. However, its role in detecting CF in HF has rarely been explored.

In this study, ^{68}Ga -FAP PET imaging was continuously performed in isoproterenol hydrochloride (ISO)-induced HF rat models to confirm its feasibility for visualizing the dynamic process of CF, and compare with histopathological staining. Then, we made a preliminary clinical exploration for recruiting HF patients to undergo ^{13}N -amino (NH_3) and ^{68}Ga -FAP PET imaging for evaluating the myocardial perfusion and fibrosis simultaneously. The aim of this study was to verify ^{68}Ga -FAP PET may offer a non-invasive imaging modality for quantifying cardiac FAP, which served as a surrogate PET biomarker for HF in clinical settings.

Materials And Methods

Animal models

The animal experiment was approved and carried out under the guidance of the animal ethics committee of Tongji Medical College, HUST. Fifty Sprague-Dawley (SD) rats (190 ± 20 g) with no specific pathogenicity were assigned to two groups: ISO-induced HF model group ($n = 25$) and the control group ($n = 25$). In the ISO-induced HF model group, rats were intraperitoneally injected with ISO (Aladdin, 5 mg/kg/day) for 14 days [20]. Rats in the control group received intraperitoneal injections of the same volume of physiological saline over the same period.

Echocardiographic assessment of cardiac function

Routine transthoracic echocardiography was performed every week before and after isoprenaline administration by two experienced operators (S He and J Wang), to verify the progress of the model and assess the left ventricular structural and functional parameters of rats. Before transthoracic echocardiography, rats were anesthetized with 1.5%–2% isoflurane to induce sedation and immobility in a supine position and at room temperature. We used Vivid E95 ultrasound machine (GE Medical Systems, Milwaukee, Wisconsin) equipped with a 12S probe at 9.0 MHz and EchoPAC workstation. At the level of the left ventricle papillary muscles, M-mode images guided by two-dimensional images of parasternal short-axis views were acquired. Left ventricular ejection fraction (LVEF), left ventricular fraction shortening (LVFS), systole left ventricle internal dimension (LVIDs), diastole left ventricle internal dimension (LVIDd), systole interventricular septal thickness (IVSs), diastole interventricular septal thickness (IVSd), systole posterior wall thickness (LVPWs), diastole posterior wall thickness (LVPWd), left ventricular end-diastolic volume (LVEDV), left ventricular end-systolic volume (LVESV), stroke volume (SV), left ventricular mass (LVM) were measured.

Preparation of ^{68}Ga -FAP and micro-PET/CT imaging of rats

The methods of synthesis and labeling of ^{68}Ga -FAP refer to those reported in the literature [21]. The experimental and control group rats were injected with ^{68}Ga -FAP (18.5 ± 0.7 MBq) *via* the tail vein on certain days (0, 7, 14, 21 and 28 d after the first injection of ISO). The microPET/CT (TransPET Discoverist 180, Raycan Technology Co., Ltd, Suzhou, China) imaging was performed after 45 min post injection with an acquisition time of 15 min. The microPET/CT images were reconstructed with the ordered-subset expectation maximization three-dimensional/maximum a posteriori probability algorithm, and then the analysis of images was done using inveon research workplace.

Tissue biodistribution and autoradiography

At 0 (before modeling), 7, 14, 21 and 28 d, experimental and control groups ($n = 3$ per group) sacrificed at 30 min after injected with ^{68}Ga -FAP (18.3 ± 0.5 MBq). The organs of interest were harvested and weighed. Radioactivity was quantified using the γ -counter (PerkinElmer, USA). The heart was then serially sectioned according to **Figure 1a** (section thickness: 2 mm) and repeat the biodistribution measurements. The biodistribution result was expressed as a percentage of the injected dose per gram of tissue (% ID/g).

Phosphor-autoradiography (ARG) was performed on the sectioned tissue immediately afterwards. Tissue slices were exposed on the phosphor screen for 15 min, followed by scanning in the Storage Phosphor Imaging System (PerkinElmer Cyclone Plus, USA) to acquire ARG images.

Histology examination

The tissues were collected for hematoxylin-eosin (H&E) and Masson's trichrome staining. Each specimen was fixed with 4% paraformaldehyde and embedded in paraffin. Immunofluorescence (IF) was applied to identify FAP expression. The fixed tissue sections were treated in methanol at -20°C for 15 min, in a serum-free blocking agent for 1 h at room temperature, and then incubated with primary antibodies for 1 h. The tissue sections were incubated in the secondary antibodies (FAP antibody, 1:200 dilution, Abcam) for 40–60 min, and mounted with Mounting Medium with 4',6-diamidino-2-phenylindole (DAPI). Image J was used to analyze the images of pathological tissues. For Masson's trichrome staining, the Collagen Volume Fraction (CVF) of myocardial tissues was calculated based on the formula: $\text{CVF} = \text{Collagen area} / \text{Total observed area} \times 100\%$. The mean gray values of the FAP protein from IF were analyzed by Image J too.

Enzyme-linked immunosorbent assay

Blood samples of rats from experimental and control groups at different time were collected from the abdominal aorta with ethylenediaminetetraacetic acid (EDTA)-K2 vacuum blood-sampling tubes and centrifuged for 15 min at $3000 \times g$ to obtain plasma. Plasma C-reactive protein (CRP), interleukin 6 (IL-6), cardiac troponin I (cTn-I), tumor necrosis factor alpha (TNF- α), angiotensin II (Ang-II) and B-type natriuretic peptide (BNP) levels were measured with commercially available enzyme-linked immunoassay (ELISA) kits (RuixinBiotech, Inc., China), according to the manufacturer's protocol.

Recruitment of HF patients

This study was approved by the Clinical Research Ethics Committee of Union Hospital, Tongji Medical College, Huazhong University of Science and Technology (NO. 20210617-01) and registered at the Clinical Trail (NCT04982458). Patients diagnosed with HF were recruited as part of this study. The inclusion criteria were shown as follows, 1) symptoms and signs of HF, 2) evidence of cardiac abnormalities, 3) age ≥ 18 y, 4) the consent of the patients, and 5) complete clinical data. Exclusion criteria were as follows: 1) acute coronary syndrome, 2) acute systemic disease or infection, uncontrolled metabolic disease, severe hepatic and renal dysfunction, 3) pregnant and lactating women. The patients had undergone both $^{13}\text{N-NH}_3$ myocardial perfusion imaging (MPI) and $^{68}\text{Ga-FAPI}$ PET scans within one day. The cardiac $^{68}\text{Ga-FAPI}$ uptake from the subjects without cardiac disease ($n = 20$, clinically confirmed) were retrospectively collected for controls.

$^{68}\text{Ga-FAPI}$ and $^{13}\text{N-NH}_3$ imaging protocol and image analysis in HF patients

For $^{13}\text{N-NH}_3$ MPI, PET acquisition (Discovery VCT, GE Healthcare) was performed immediately after intravenous injection of $^{13}\text{N-NH}_3$ (370–740 MBq) with an acquisition time of 10 min. Two hours after completing $^{13}\text{N-NH}_3$ MPI, $^{68}\text{Ga-FAPI}$ (1.8–2.2 MBq/kg) was injected intravenously. $^{68}\text{Ga-FAPI}$ imaging was performed for 20 min at 45 min time points according to the previous method [22]. Attenuation-corrected PET images were reconstructed using ordered-subset expectation maximization iterative method. The gated data were reconstructed by volume image protocol (VIP) replay. $^{13}\text{N-NH}_3$ perfusion and $^{68}\text{Ga-FAPI}$ imaging were further processed using Emory Cardiac Toolbox in Xeleris Workstation (2.0, GE Healthcare). The PET indices of $^{68}\text{Ga-FAPI}$ (maximum standardized uptake value [SUV_{max}], mean standardized uptake value [SUV_{mean}] and SUV_{max} of myocardium / cardiocoelomic SUV_{mean} [Normalized- SUV_{max}]) were acquired by Advanced Workstation (AW4.6, GE Healthcare).

Statistical analysis

Data were expressed as mean \pm standard deviations (SD). Statistical analysis was performed using analysis of variance (ANOVA) and Student's t -test with commercial software (GraphPad Prism 8 and SPSS 13.0). $P < 0.05$ indicates statistical significance.

Results

Sequential $^{68}\text{Ga-FAPI}$ phosphor-autoradiography and histopathology in HF rat models

The hearts were dissected and sliced into consecutive sections as shown in Fig. 1a. For HF rats with modeling, the phosphor-autoradiography images displayed continuously increased $^{68}\text{Ga-FAPI}$ uptakes (Fig. 1b) at 7 d and 14 d, and gradually decreased at 21 d and 28 d. Furthermore, cardiac radioactivity in the coronal section was significantly reduced from apical cordis to basal cordis. To verify the myocardial fibrosis of HF progression, the heart of the rats from different periods were sliced and examined by H&E, Masson's and

FAP IF staining (Fig. 1c). The results showed that fibrosis aggravates during the progress of ISO-induced HF model. And IF staining revealed FAP expression reached its peak at 7 d, and continue to express on the 14 d. However, the expression decreased on the 21 d, and no obvious signal was detected on the 28 d.

Sequential ^{68}Ga -FAPI images in HF model

No obvious ^{68}Ga -FAPI accumulations (Fig. 2a) were observed in the myocardium at 0 d and control groups' rats. With the development of the ISO-induced HF model, extensive uptake of the myocardium was observed on ^{68}Ga -FAPI PET imaging. It peaked at 7 d after the HF model, accompanied by increased ventricular systolic function. Subsequently, it showed gradual decreases in myocardial uptake from 14 to 28 d. As HF progresses, ventricular systolic function aggravated verified by echocardiography (Fig. 2b). As shown by M-mode ultrasound, the ventricular wall thickening reached its peak, the amplitude of ventricular wall motion increased, and the myocardial contraction was enhanced at 7 d. Subsequently, the heart chambers of rats gradually expanded, the thickness of ventricular wall gradually decreased, the amplitude of ventricular wall motion gradually decreased, and the myocardial contraction gradually weakened.

Cardiac dysfunction of rats in ISO-induced models

Myocardial functions were evaluated by echocardiography (Fig. 3). Along with modeling progress, LVEF, LVFS, LVPWd, LVPWs, IVSd, IVSs, and LVM (Fig. 3a-g) significantly increased at 7 d and then gradually decreased, implying a decrease in ventricular systolic function after excessive compensatory. However, LVEDV, LVESV, SV, LVIDd, LVIDs and cardiac volume (Fig. 3h-l) significantly decreased at 7 d after injection of ISO and then appeared with an increasing trend.

Cardiac enzyme-linked immunosorbent assay in HF models

Circulating levels of BNP, cTn-I, CRP, Ang-II, IL-6 and TNF- α were measured as cardiac-related serological indicators. The BNP levels (Fig. 4a) slightly increased in 14 d compared to 0 d with statistical significance. Importantly, significantly higher plasma cTn-I, CRP, Ang-II and IL-6 levels (Fig. 4b-e) were shown in both 14, 21 and 28 d compared to 0 d. Although, the TNF- α levels (Fig. 4f) in 21 and 28 d were significantly higher than 0 d.

In vitro biodistribution and pathological section statistical analysis of ISO models

At the initiation (0 d), there was no significant difference in cardiac uptake of ^{68}Ga -FAPI among the myocardial layers. The heart-to-muscle (H/M) ratios of ^{68}Ga -FAPI (Fig. 5a) was highest on 7 d, and then gradually decreased. The highest concentrated site was Heart 5 (apex cordis) section, with H/M ratios and uptake values of 19.97 ± 0.33 and $0.61 \pm 0.07\% \text{ID/g}$ at 7 d (**S**. Tables 1 and 2), respectively.

Table 1
Clinical characteristics of enrolled patients

| No. | Age, y | Gender | Time [#] | CRD | Cardiac operation | Family history | ¹³ N-NH ₃ MPI | | | ⁶⁸ Ga-FAPI | |
|-----|--------|--------|-------------------|----------------------|-------------------|----------------|-------------------------------------|-----|-------------------------------------|------------------------|----------------------------------|
| | | | | | | | LVEDV | EF | Characteristic | Nor-SUV _{max} | Characteristic |
| 1 | 72 | Female | 1 mo | DCM | - | CHD | 224 mL | 23% | Slightly uneven decrease | 9.00 | Diffuse uptake |
| 2 | 46 | Male | 9 mo | CHD, arrhythmia | PCI, ICD, RFA | DCM | 243 mL | 15% | Slightly decrease with local defect | 8.83 | Diffuse uptake with local defect |
| 3 | 31 | Male | 2 mo | - | Myocarditis | - | 162 mL | 12% | Uneven decrease | 5.75 | Diffuse uptake |
| 4 | 61 | Female | 1.3 y | HCM | - | HCM | 106 mL | 38% | Mild uneven decrease | 5.00 | Diffuse uptake |
| 5 | 75 | Male | 4 y | CHD | PCI | - | 117 mL | 31% | Mild diffuse decrease | 3.78 | Diffuse uptake |
| 6 | 71 | Male | 5.5 y | CHD, arrhythmia | ICD, PCI | - | 120 mL | 32% | Mild decrease with local defect | 3.08 | Slight uptake |
| 7 | 51 | Male | 12 y | Diabetes, arrhythmia | ICD | DCM | 161 mL | 29% | Severely uneven decrease | 2.57 | Slight uptake |

[#] means clinically diagnosed time, mo refers to month, y refers to year; CRD: History of cardiovascular related diseases; Nor-SUV_{max}: Normalized-SUV_{max} (SUV_{max} of myocardium / cardiocoelomic SUV_{mean}); CHD: Coronary heart disease; PCI: Percutaneous coronary intervention; ICD: Implantable cardioverter defibrillator; RFA: Radio frequency ablation; DCM: Dilated cardiomyopathy; HCM: Hypertrophic cardiomyopathy.

The correlation between H/M ratios of Heart 5 and mean gray value of FAP (Pearson correlation, $P < 0.0001$; $R^2 = 0.879$) was shown in Fig. 5b. The mean gray values (blue line, Fig. 5c) at 7 d (101.76 ± 2.98 , $P < 0.0001$) and 14 d (90.69 ± 4.42 , $P = 0.0002$) were both higher than 0 d (78.89 ± 1.36). The CVF (red line, Fig. 5c) collected from the Masson's staining were gradually increased with modeling time, and was significantly higher than 0 d (0.31 ± 0.13) at 14, 21 and 28 d (6.31 ± 0.19 , 15.69 ± 2.19 and 19.19 ± 5.05 , respectively).

⁶⁸Ga-FAPI and ¹³N-NH₃ imaging in patients with HF

Seven patients with clinically diagnosed as HF were successfully recruited (5 men and 2 women, the average age was 58.14 ± 16.25 years old, Table 1). ⁶⁸Ga-FAPI was found to show varying levels of cardiac uptake in patients with HF (Fig. 6a). Higher cardiac ⁶⁸Ga-FAPI uptake was demonstrated in the patients with < 1-year duration (Table 1, $n = 3$, Normalized-SUV_{max}: 7.86 ± 1.83) than patients > 1-year ($n = 4$, Normalized-SUV_{max} [SUV_{max} of myocardium / cardiocoelomic SUV_{mean}]: 3.61 ± 1.53 , $P = 0.011$) and patients without cardiac disease ($n = 20$, 1.24 ± 0.25 , $P = 0.024$). ¹³N-NH₃ MPI displayed with different types of decrease, and remarkably in the patients with duration > 3-year.

Two patients (No. 1 and 2) were selected to demonstrate the characteristics of ⁶⁸Ga-FAPI and ¹³N-NH₃ imaging (Fig. 6b and c). A 72-year-old female (Case 1) had precordial discomfort and shortness of breath for one month. She also has a history of congestive dilated cardiomyopathy. Echocardiography showed reduced left ventricular wall motion and enlarged left heart with a LVEF value of 25%. ¹³N-NH₃ PET showed varying reduced myocardial perfusion in apex, middle segment, base segments of the left ventricle. Avid accumulation of ⁶⁸Ga-FAPI were observed in the left ventricle, especially in the anterior and inferior walls (Normalized-SUV_{max}: 9.0). A 46-year-old male (Case 2) has a history of coronary heart disease. Recently, post-activity asthma had occurred and gradually progressive for 9 months. Echocardiography showed enlargement of left heart with a LVEF value of 24%. In ¹³N-NH₃ PET, large defect in the distribution of imaging agents in the left ventricular septum. However, ⁶⁸Ga-FAPI PET showed obvious aggregation in the anterior and inferior wall with Normalized-SUV_{max} of 8.89. The combination of ¹³N-NH₃ and ⁶⁸Ga-FAPI bull's eye diagram showed that ¹³N-NH₃ perfusion was inconsistent with ⁶⁸Ga-FAPI uptake, and partial defect supplement imaging presented. ⁶⁸Ga-FAPI accumulation distribute widely in

ventricle with different degrees, remarkable in anterior and inferior walls. This is thought to be an active expression of FAP at this stage, which is further involved in ventricular remodeling. In Case 1, $^{13}\text{N-NH}_3$ perfusion displayed with slightly uneven decrease. In Case 2, both defects of $^{13}\text{N-NH}_3$ and $^{68}\text{Ga-FAPI}$ PET were shown in part of left ventricular septum, implying the area as infarction. $^{13}\text{N-NH}_3$ perfusion was deficient in part of apex and proximal apex with moderate FAPI expression, suggesting the area as severe ischemia but FAP active.

Discussion

In this study, we successfully built ISO-induced HF rat models, and applied $^{68}\text{Ga-FAPI}$ PET to visualize the CF and monitor the progress of HF. It demonstrates that $^{68}\text{Ga-FAPI}$ accumulated in the heart and reached peak at 7 d after modeling, then decreased with the process of HF. The uptakes of $^{68}\text{Ga-FAPI}$ had good correlations with the myocardial Masson and FAP IF staining. We also recruited HF patients for $^{68}\text{Ga-FAPI}$ PET imaging, which showed higher myocardium uptake of HF patients with a shorter duration, but gradually decreased with the extension of the course of disease. These preliminary results suggested that $^{68}\text{Ga-FAPI}$ PET may visualize the process of fiber activation in the early stage of HF, while the fibrosis has been formed in the late stage, and $^{68}\text{Ga-FAPI}$ PET was not recommended for evaluation. Furthermore, these results gave the hypothesis that $^{68}\text{Ga-FAPI}$ PET may help for seeking patients with early HF or in the active stage of fibrosis, to facilitate the treatment decisions.

At present, cardiac remodeling is considered one of the most important clinical determinants of the progression of HF [23]. It has typical molecular, cellular, and extracellular changes, clinically manifested as variations in heart size, shape, and function [24]. The pathophysiology and underlying cellular processes that drive cardiac remodeling are not caused by a loss of cardiomyocytes or focal myocardial injury, but instead a pervasive and global fibroblast proliferation and development of fibrosis [25]. Therefore, the detection of the process and degree of fibrosis is expected to understand the stage of cardiac remodeling, and further explore the degree of HF. It may also provide a basis for early clinical prevention and treatment of HF. FAP is highly expressed in activated fibroblasts, and it has been studied and applied to reflect the fibrosis process of diseases [26].

Our study sought to discover the value of $^{68}\text{Ga-FAPI}$ PET in HF. The ISO-induced HF models were successfully built. Cardiac uptake of $^{68}\text{Ga-FAPI}$ peaked at 7 d, and then gradually decreased. It was confirmed by ARG and immunoprotein staining *ex vivo*, which demonstrated that $^{68}\text{Ga-FAPI}$ could visualize dynamical changes of FAP protein [27, 28]. Cardiac function reached its maximum at 7 d and then decreased for limitation of irreversible damage, which is similar to the $^{68}\text{Ga-FAPI}$ uptake. Different from the changes of FAP protein, histological validation of CVF revealed that myocardial fibrosis started at 14 d, and gradually developed over time. Similarly, ventricular load, necrosis of myocardial cells and inflammation of the cardiovascular system gradually aggravated since 14 d after modeling, as reflected by serological indicators. Therefore, a large area of avid FAP expression may subsequently triggers extensive fibrosis of the myocardium, aggravating the degree of HF. Benefit from this, active FAP expression may also serve as an indicator for early anti-ventricular remodeling treatment. Thus, $^{68}\text{Ga-FAPI}$ can be a useful tool to early visualize HF progress and assess the efficacy of antifibrotic therapy.

To evaluate its clinical translation potential, 7 patients with HF were enrolled to get $^{68}\text{Ga-FAPI}$ and $^{13}\text{N-NH}_3$ imaging. It confirmed FAP expression in clinical HF patients, and $^{68}\text{Ga-FAPI}$ is sensitive for detection of active fibrosis existence. In addition, $^{68}\text{Ga-FAPI}$ uptake was inconsistent with $^{13}\text{N-NH}_3$ perfusion, identifying the two probes can visualize two imaging events (myocardial perfusion and activated cardiac fibroblasts) in one stop. Patients with short disease duration presented with avid $^{68}\text{Ga-FAPI}$ accumulation, and gradually decreased in patients with advanced disease. This may stem from the fact that patients with short disease duration are closely related to the origin of ventricular remodeling, serving as indirect evidence of fibroblast activation and predictor of cardiac fibroblasts. In addition, infarcted myocardium demonstrates both negative uptake in $^{68}\text{Ga-FAPI}$ and $^{13}\text{N-NH}_3$ imaging. In areas with active FAP expression, where $^{13}\text{N-NH}_3$ perfusion defect may indicate the sites as severe ischemia but FAP active, also may indicate further involvement in ventricular remodeling and pro-fibrotic activity.

We realize that there were several limitations in our study. First, this study was restricted to a limited number of HF patients, which limits effective classification of HF patients. Second, the enrolled patients have been clinically diagnosed with HF, while the rat models reflect the whole process of HF. At the same time, different from a single type of positive inotropic HF in rats, the pathological classifications of HF patients are various, which may lead to partly inconsistency in patients and rat models. Furthermore, anti-ventricular remodeling treatment need to further investigate to identify the clinical role of FAP in HF patients. The value of such imaging indicator should be confirmed in larger prospective studies.

Conclusion

With the progress of HF, ^{68}Ga -FAP accumulates evidently in the early stage, and gradually reduced to almost indiscernible. Active FAP expression prompts myocardial remodeling and subsequent fibrosis of the myocardium. Early active FAP expression may serve as an indicator for anti-ventricular remodeling treatment. Preliminary studies suggest that ^{68}Ga -FAP PET can be used to display active fibrosis, which has clinical significance for guiding the decision of anti-fibrosis drug therapy.

Declarations

Disclosures

The authors declare that they have no conflict of interest.

Funding

This work was financially supported by National Natural Science Foundation of China (grants 82030052).

Ethical approval

This study was approved by the Clinical Research Ethics Committee of Union Hospital, Tongji Medical College, Huazhong University of Science and Technology (NO. 20210617-01) and registered at the Clinical Trail (NCT04982458).

Consent to participate and publication

The requirement for informed consent was waived.

Availability of data and code

Not applicable.

Authors' contributions

X. L. conceived and designed the study devised, supervised the project. X. Z. and W. S. finished the animal experiments and wrote the manuscript. J. W. and S. H. performed routine transthoracic echocardiography. Y. G. synthesized the probe. C. Q. and F. H. analyzed the image data. Y. W., Z. W. and P. B. contributed to patient clinical data analysis.

Funding Sources

This work was financially supported by National Natural Science Foundation of China (82030052).

References

1. Ponikowski P, Voors AA, Anker SD, et al. 2016 ESC Guidelines for the diagnosis and treatment of acute and chronic heart failure: The Task Force for the diagnosis and treatment of acute and chronic heart failure of the European Society of Cardiology (ESC). Developed with the special contribution of the Heart Failure Association (HFA) of the ESC. *Eur Heart J*. 2016;37:2129–200.
2. Global regional. and national incidence, prevalence, and years lived with disability for 354 diseases and injuries for 195 countries and territories, 1990–2017: a systematic analysis for the Global Burden of Disease Study 2017. *Lancet*. 2018;392:1789–858.
3. Von Schwarz ER, He M, Bharadwaj P. Palliative care issues for patients with heart failure. *JAMA Netw Open*. 2020;3:e200011–1.
4. Mamas MA, Sperrin M, Watson MC, et al. Do patients have worse outcomes in heart failure than in cancer? A primary care-based cohort study with 10-year follow-up in Scotland. *Eur J Heart Fail*. 2017;19:1095–104.
5. Mohebbi D, Kittleson MM. Remote monitoring in heart failure: current and emerging technologies in the context of the pandemic. *Heart*. 2021;107:366–72.
6. Travers JG, Kamal FA, Robbins J, Yutzey KE, Blaxall BC. Cardiac fibrosis: the fibroblast awakens. *Circ Res*. 2016;118:1021–40.
7. Kong P, Christia P, Frangogiannis NG. The pathogenesis of cardiac fibrosis. *Cell Mol Life Sci*. 2014;71:549–74.
8. Kim GH, Uriel N, Burkhoff D. Reverse remodelling and myocardial recovery in heart failure. *Nat Reviews Cardiol*. 2018;15:83–96.
9. Aghajanian H, Kimura T, Rurik JG, et al. Targeting cardiac fibrosis with engineered T cells. *Nature*. 2019;573:430–3.

10. Liu T, Song D, Dong J, et al. Current understanding of the pathophysiology of myocardial fibrosis and its quantitative assessment in heart failure. *Front Physiol.* 2017;8:238.
11. Heckmann MB, Reinhardt F, Finke D, et al. Relationship between cardiac fibroblast activation protein activity by positron emission tomography and cardiovascular disease. *Circ Cardiovasc Imaging.* 2020;13:e010628.
12. Quittner AL, Eakin MN, Alpern AN, et al. Clustered randomized controlled trial of a clinic-based problem-solving intervention to improve adherence in adolescents with cystic fibrosis. *J Cyst Fibros.* 2019;18:879–85.
13. Kuchulakanti PK. ARNI in cardiovascular disease: current evidence and future perspectives. *Future Cardiol.* 2020;16:505–15.
14. Lewis GA, Dodd S, Clayton D, et al. Pirfenidone in heart failure with preserved ejection fraction: a randomized phase 2 trial. *Nat Med.* 2021;27:1477–82.
15. Vagnozzi RJ, Johansen AKZ, Molkentin JD. CARdiac immunotherapy: T cells engineered to treat the fibrotic heart. *Mol Ther.* 2019;27:1869–71.
16. Zhang X, Song W, Qin C, Liu F, Lan X. Non-malignant findings of focal (68)Ga-FAPI-04 uptake in pancreas. *Eur J Nucl Med Mol Imaging.* 2021;48:2635–41.
17. Qin C, Shao F, Gai Y, et al. (68)Ga-DOTA-FAPI-04 PET/MR in the evaluation of gastric carcinomas: comparison with (18)F-FDG PET/CT. *J Nucl Med.* 2022;63:81–8.
18. Röhrich M, Leitz D, Glatting FM, et al. Fibroblast activation protein-specific PET/CT imaging in fibrotic interstitial lung diseases and lung cancer: a translational exploratory study. *J Nucl Med.* 2022;63:127–33.
19. Yuan T, Wang X. 68Ga-FAPI PET/MRI in coronary heart disease. *J Nucl Cardiol* 2021.
20. Zhang XJ, Tan H, Shi ZF, Li N, Jia Y, Hao Z. Growth differentiation factor 11 is involved in isoproterenol-induced heart failure. *Mol Med Rep.* 2019;19:4109–18.
21. Loktev A, Lindner T, Mier W, et al. A tumor-imaging method targeting cancer-associated fibroblasts. *J Nucl Med.* 2018;59:1423–9.
22. Siebermair J, Köhler MI, Kupusovic J, et al. Cardiac fibroblast activation detected by Ga-68 FAPI PET imaging as a potential novel biomarker of cardiac injury/remodeling. *J Nucl Cardiol.* 2021;28:812–21.
23. Azevedo PS, Polegato BF, Minicucci MF, Paiva SAR, Zornoff LAM. Cardiac remodeling: concepts, clinical Impact, pathophysiological mechanisms and pharmacologic treatment. *Arq Bras Cardiol.* 2016;106:62–9.
24. Cohn JN, Ferrari R, Sharpe N. Cardiac remodeling—concepts and clinical implications: a consensus paper from an international forum on cardiac remodeling. Behalf of an international forum on cardiac remodeling. *J Am Coll Cardiol.* 2000;35:569–82.
25. Talman V, Ruskoaho H. Cardiac fibrosis in myocardial infarction—from repair and remodeling to regeneration. *Cell Tissue Res.* 2016;365:563–81.
26. Fan M-H, Zhu Q, Li H-H, et al. Fibroblast activation protein (FAP) accelerates collagen degradation and clearance from lungs in mice. *J Biol Chem.* 2016;291:8070–89.
27. Varasteh Z, Mohanta S, Robu S, et al. Molecular imaging of fibroblast activity after myocardial infarction using a 68Ga-labeled fibroblast activation protein inhibitor, FAPI-04. *J Nucl Med.* 2019;60:1743–9.
28. Notohamiprodjo S, Nekolla SG, Robu S, et al. Imaging of cardiac fibroblast activation in a patient after acute myocardial infarction using 68Ga-FAPI-04. *J Nucl Cardiol* 2021.

Figures

Figure 1

⁶⁸Ga-FAPI phosphating autoradiography observation of continuous myocardial layers and histopathological results at different periods in ISO-induced HF model. (a) The schematic diagram of cardiac sliced sections. (b) ⁶⁸Ga-FAPI phosphating autoradiography of the sections during the HF progression (0, 7, 14, 21 and 28 d). (c) Representative H&E, Masson's, and FAP IF staining (FAP, red; DAPI, blue) of the heart tissues at the corresponding periods.

Figure 2

A series of sequential ^{68}Ga -FAPI tomographic images of ISO-induced HF model and control group at 0, 7, 14, 21 and 28 d. (a) ^{68}Ga -FAPI coronal plane of ISO and control group (b) Transthoracic echocardiography image of ISO group. Red arrows refer to the heart, yellow arrows refer to LVIDd, and green arrows refer to LVIDs.

Figure 3

Cardiac structural and functional parameters. The parameters were measured by transthoracic echocardiography in the ISO-induced HF model rats, namely left ventricular ejection fraction (LVEF), left ventricular fraction shortening (LVFS), diastole posterior wall thickness (LVPWd), systole posterior wall thickness (LVPWs), diastole interventricular septal thickness (IVSd), systole interventricular septal thickness (IVSs), left ventricular mass (LVM), left ventricular end-diastolic volume (LVEDV), left ventricular end-systolic volume (LVESV), stroke volume (SV), diastole left ventricle internal dimension (LVIDd) and systole left ventricle internal dimension (LVIDs) ($n = 5$). Graphs represent mean \pm SD. *, $P < 0.05$; **, $P < 0.01$; ***, $P < 0.001$, compared with 0 d group.

Figure 4

Cardiac hormone secretion indicators levels. Plasma BNP (a), cTn-I (b), CRP (c), Ang-II (d), IL-6 (e) and TNF- α (f) levels in different time (0, 7, 14, 21 and 28 d) were expressed as mean \pm SD in the graphic. * refers to $P < 0.05$; ** refers to $P < 0.01$; *** refers to $P < 0.001$, compared with 0 d group.

Figure 5

Quantitative analysis of HF models. (a) Heart-to-muscle (H/M) uptake ratios at different time (0, 7, 14, 21 and 28 d) and sections (Heart 1-5 and total). (b) Linear plots of collagen volume fraction (CVF) and mean grey value over time (red, CVF; blue, mean grey value). (c) Correlation analysis between H/M ratios of Heart 5 and mean grey value (green dots, variables). The cross section of heart section is shown in **Figure 1a**. * refers to the ratio of H/M in the same section with 0 d. * refers to $P < 0.05$; ** refers to $P < 0.01$; *** refers to $P < 0.001$; **** refers to $P < 0.0001$. + refers to different group compared with 0 d group. +, $P < 0.05$; ++, $P < 0.01$; +++, $P < 0.001$; +++, $P < 0.0001$.

Figure 6

^{68}Ga -FAPI and ^{13}N - NH_3 images in patients without cardiac disease and with HF. (a) Axial ^{68}Ga -FAPI PET/CT imaging of heart in control subjects (without cardiac disease) and HF patients with different duration. ^{13}N - NH_3 perfusion and ^{68}Ga -FAPI PET Bullseye plot and short axis serial images in patient No. 1 (b) and 2 (c), respectively.

Supplementary Files

This is a list of supplementary files associated with this preprint. Click to download.

- [SupportingInformation.docx](#)